Proceedings of the ASME 2010 3rd Joint US-European Fluids Engineering Summer Meeting and 8th International Conference on Nanochannels, Microchannels, and Minichannels
FEDSM-ICNMM2010
August 1-5, 2010, Montreal, Canada

FEDSM-ICNMM2010-30031

LOWER ENTROPY GENERATION IN MICROCHANNELS WITH LAMINAR SINGLE PHASE FLOW

Galvis E.
University of Waterloo
Waterloo, Ontario, Canada
N2L 3G1

Culham J. R.
University of Waterloo
Waterloo, Ontario, Canada
N2L 3G1

ABSTRACT

In this study the entropy generation minimization method is used to find the optimum channel dimensions in micro heat exchangers with a uniform heat flux. With this approach, pressure drop and heat transfer in the micro channels are considered simultaneously during the optimization analysis. A computational model is developed to find the optimum channel depth knowing other channel geometry dimensions and coolant inlet properties. The flow is assumed laminar and both hydrodynamically and thermally fully developed and incompressible. However, to take into account the effect of the developing length in the friction losses, the Hagenbach's factor is introduced. The micro channels are assumed to have an isothermal or isoflux boundary condition, non-slip flow, and fluid properties have dependency on temperature accordingly.

For these particular case studies, the pressure drop and heat transfer coefficient for the isoflux boundary condition is higher than the isothermal case. Higher heat transfer coefficient and pressure drop were found when the channel size decreased. The optimum channel geometry that minimizes the entropy generation rate tends to be a deep, narrow channel.

NOMENCLATURE

A	Channel wetted area, m^2, channel cross section area, m^2
a	Channel width, *m*
b	Channel depth, *m*
c_p	Specific heat, *J/kgK*
d_h	Hydraulic diameter ($4A_c/P$), *m*
f	Friction factor coefficient
h	Heat transfer coefficient, W/m^2K, enthalpy, *J/kg*
K	Hagenbach's factor
k	Thermal conductivity, *W/mK*
L	Channel length, *m*
m	Fin parameter, m^{-1}
$\dot{m}$	Flow rate, *m/s*
n	Number of channels
Nu	Nusselt number $\equiv hd_h/k_f$
P	Channel perimeter, *m*
p	Pressure, *Pa*
$\dot{Q}$	Heat flow rate, *W*
q	Heat flux, W/m^2
R	Thermal resistance, *K/W*
Re	Reynolds number $\equiv Vd_h/\nu$
$\dot{S}_{gen}$	Rate of entropy generation, *W/K*
s	Entropy, *J/kgK*, channel wall thickness, *m*
T	Temperature, *K*
t	Time, *s*
u	Internal energy per unit mass, *J/kg*
V	Velocity ($u, v=0, w=0$), *m/s*
W	Micro heat exchanger width, *m*

Greek symbols

α	Channel aspect ratio $\equiv b/a$
η_f	Fin efficiency
μ	Dynamic viscosity, *Pa.s*
ν	Kinematic viscosity, m^2/s
ρ	Fluid density, kg/m^3
Δp	Pressure drop, *Pa*

Subscripts

a	Ambient
app	Apparent
ave	Average
c	Channel
cv	Control volume
f	Fluid, fin
gen	Generated
in	Entrance
max	Maximum
out	Exit
opt	Optimum
s	Wall

INTRODUCTION

The efficiency of a Micro Heat Exchanger (MHE) is determined as a function of its thermal resistance, which is the sum of the resistance against conduction in the substrate and other laminated structures, the resistance against convection from the substrate to the flow, and the resistance due to the absorption of heat by the fluid. The conductive resistance is usually very small and the resistance due to the heating of the fluid can be reduced by using a coolant of high specific heat capacity and high volume flow rate. The only resistance that can not be conveniently reduced is the convective resistance, also known as the film resistance. This term is the dominant and thus the controlling term in the resistance network. Since the film resistance is proportional to the inverse of the product of the heat transfer coefficient and the wetted surface area, the film resistance can be minimized through an increase of either of these design parameters. The wetted surface area can be increased by creating channels for the flow in the substrate. Assuming fully developed flow (thus Nusselt number does not vary along the channel), constant fluid properties, and noting an inverse relationship between heat transfer coefficient and channel dimension ($h=Nuk_f/d_h$), the best way to obtain significantly high convection heat transfer coefficient is to use microscopic channels. However, since smaller channel sizes are associated with higher pressure drops, it is necessary to calculate an optimum channel size that simultaneously minimizes the film resistance ($R_{film}=1/hA$) and flow resistance ($R_{flow}=1/\dot{m}\, c_p$).

The optimization of fluid devices, both thermally and hydrodynamically, can be achieved by minimizing the entropy generation. In this study, an entropy generation minimization method is employed to optimize the overall performance of the MHE. There are very few papers that adopt a second law approach to this problem. Khan et al. [1] employed an entropy generation model to optimize the overall performance of microchannel heat sinks. Microchannel width, height and fin thickness were optimized in terms of channel aspect ratio and fin spacing ratio for three different volume flow rates and Knudsen numbers in the slip flow region. They employed analytical-numerical correlations for the pressure drop and heat transfer in microchannels, with the hydraulic diameter used as the characteristic length. Also, a fin approach was used to develop a model for the thermal resistance, assuming adiabatic fin tips and correlations developed for conventional, large channels for the pressure drop. They observed that both channel aspect and fin spacing ratios increase with an increase in volumetric flow rate. Also, the thermal resistance and pressure drop were found to decrease with an increase in volumetric flow rate, and increase with a decrease in Knudsen numbers in the slip flow region. In addition, they also found that narrow channels tentd to give the lowest entropy generation rate. Chen [2] used the second law of thermodynamics to optimize microchannels under different thermal boundary conditions. He considered heat conduction in the flow direction but entrance effects and friction losses in the microchannel were neglected. The local entropy generation rate was found to be only dependent upon the temperature gradient in the flow direction. The significant shortcoming of this study is neglecting the frictional effect in the analysis.

Abbassi [3] analyzed a uniformly heated micro heat exchanger using a porous media approach in order to investigate local entropy generation as a criterion for assessing system performance. The second law analysis was conducted on the basis of obtained velocity and temperature fields and expressions for local and average entropy generation rate were derived in dimensionless form. He found that the entropy generation rate is a strong function of channel aspect ratio, thermal conductivity ratio, Brinkmann number, and porosity and it is only a weak function of Peclet number for common applications. This work concludes that entropy generation has an optimum value for aspect ratio; whereas thermal entropy generation decreases and pressure drop rises with increasing aspect ratio.

In terms of the friction factor and heat transfer rate in microchannels, fundamental investigations have been conducted by many researches, generally using theoretical values developed from the Navier-Stokes and energy equations. In fact, a number of publications have shown that experimental results at the micro scale were lower, higher or in some cases similar to theoretical values, indicating that the Navier-Stokes and energy equations by themselves are incapable of modeling the governing physical mechanisms inside the microchannels.

Several effects, which are normally neglected when considering macro scale flow, may be significant at the micro scale. As the characteristic lengths are reduced to the same order of magnitude as the hydrodynamic boundary layer thickness, momentum transfer in directions other than the streamwise direction can increase significantly. Sources of error in micro scale fluid experiments may have a number of inherent problems that can lead to undetectable errors, undesirable levels of uncertainty, and complications in comparing experimental results to traditional theory. These experimental difficulties may be related to measurements of the channel dimensions, pressure drop and flow rate and the surface effect introduced by surface roughness. Also, temperature variations in the transport fluid may cause a significant variation in fluid properties.

Zheng and Silber-Li [4] measured 14 horizontal profiles along the vertical direction of a rectangular microchannel with an aspect ratio 0.35. They found that the experimental velocity profiles are in agreement with the theoretical profiles except for planes close to the wall. Papautski et al. [5] presented a summary of experimental research efforts in the area of microscale single phase internal flow and discussed issues associated with investigating microscale flows. The only definitive conclusion that was reached is that slip flow gas data indicated an approximately 60% reduction in the friction factor compared to macroscale theory at the same Reynolds number. Results for other types of flows (water, alcohol) are inconclusive as they appear both above and below the theoretical prediction. Papautski et al. [6] evaluated the effects of rectangular microchannel aspect ratio on the laminar friction factor. The experimental data obtained for water flows indicated an approximately 20% increase in the laminar friction factor for a specified flow rate when compared to the macroscale prediction from the classical Navier-Stokes theory.

A resent study for Park and Punch [7] focused on laminar flow (69<Re<800) within rectangular microchannels with hydraulic diameters from 106 μm to 307 μm for single phase liquid flow. The study showed that the friction factors obtained by experiments are in good agreement with the conventional theory for fully developed flow within the range of their experiments. However, a deviation between the experimental and theoretical values of heat transfer rate in the microchannels was found.

This paper provides a mathematical model for the heat transfer, pressure drop and optimization of the channel aspect ratio in a MHE having straight channels with isothermal or isoflux boundary condition. Entropy generation minimization is proposed as a method to optimize the channel width. Also, the effect of the channel size, and some design parameters such as MHE size, channel wall and heat flux are studied.

MODEL AND ASSUMPIONS

The schematic diagram of a representative Micro Heat Exchanger (MHE) is presented in Figure 1. The upper surface is properly insulated and heat flux q is applied from the vertical direction through the lower plate and coolant flow is parallel to the x direction. The flow is assumed laminar and both hydrodynamically and thermally fully developed and incompressible. However, to take into account the effect of the developing length in the friction losses, the Hagenbach's factor was introduced. Radiative heat transfer is neglected.

The channel dimensions are expressed with channel width a, channel depth b, wall thickness s between the channels, and overall width W and length L.

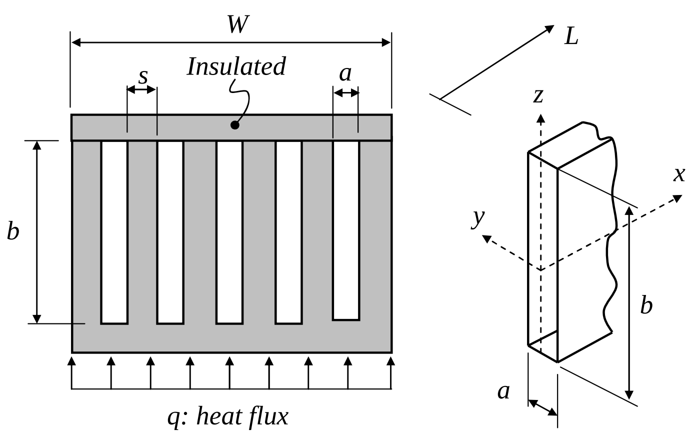

Figure 1: Schematic MHE

The number of channels n is calculated based on the MHE width (W), the channel width (a) and wall thickness (s).

$$n = \frac{W - s}{a + s}$$

The governing equations were solved based on the following assumptions:

- Spatial variation and dependency with time in density are negligible.
- Steady state, 2-D fully developed laminar non-slip flow, and negligible body forces.
- Fully developed heat flow.
- Uniform heat flux on the bottom surface.
- Isotropic material, smooth surface of the channel, and adiabatic fin tips.
- Thermal properties of the fluid depend on temperature.
- Negligible axial conduction in both the fin and fluid.
- Changes in kinetic and potential energies negligible.
- Zero internal heat generation, negligible viscous dissipation, and compressibility effects.

The value for Nusselt number Nu is obtained from Kakac et al. [8] for constant wall temperature T_s at all four walls of a rectangular channel.

$$Nu = 7.541(1 - 2.610\alpha + 4.970\alpha^2 - 5.119\alpha^3 + 2.702\alpha^4 - 0.548\alpha^5)$$

where α is the channel aspect ratio b/a.

The heat transfer coefficient h can now be calculated based on the Nu, the thermal conductivity of the fluid k_f and the hydraulic diameter $d_h=4ab/[2(a+b)]$

$$h \equiv Nu \frac{k_f}{d_h}$$

Note that the temperature inlet of the fluid T_{in} is known and the temperature of the fluid outlet T_{out} is unknown. For that reason the properties of the fluid were initially estimated at average temperature: $(T_{in}+T_{max})/2$. T_{max} was considered as the maximum allowable chip temperature. As soon as T_{out} is known, all the properties of the fluid were recalculated at $(T_{in}+T_{out})/2$.

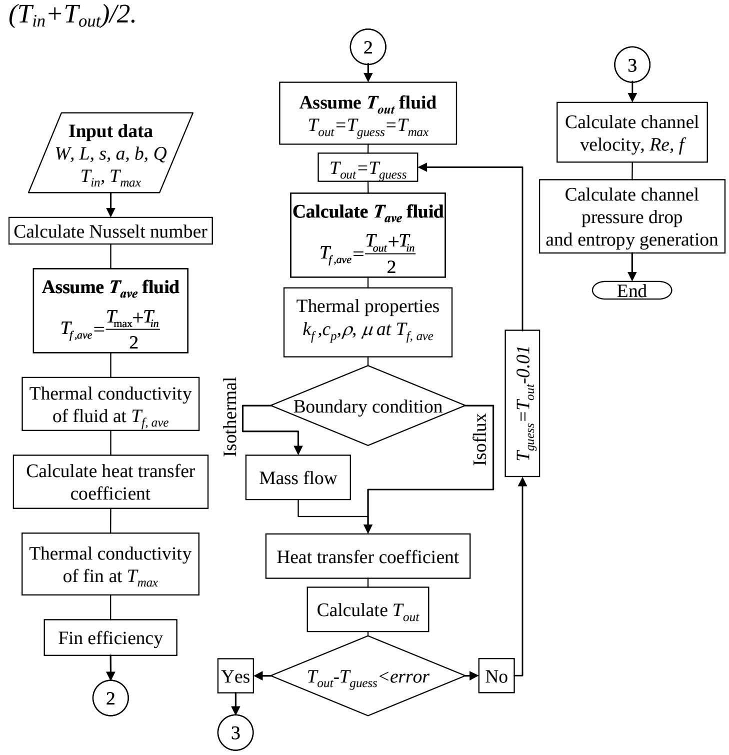

Figure 2: Flow chart for the mathematical model

A similar methodology as proposed by Upadhye and Kandlikar [9] was used to calculate the temperature leaving the channel (T_{out}). The iterative technique is shown in the chart flow in Figure 2 and explained as follow: The first mathematical process is the calculation of the fin efficiency which is approximately between 80 and 99% for the cases studied in this paper.

The second mathematical process in the flow chart is the calculation of the temperature of the fluid leaving the micro channels. The temperature of the fluid leaving the channel was assumed to be $(T_{out})_{guess}=T_{max}$. Once the temperature of the fluid leaving the channel is "known", the mass flow rate $\dot{m}$ can be calculated from.

$$\dot{m} = \frac{\dot{Q}}{c_p (T_{out} - T_{in})}$$

where $\dot{Q}$ is the desired heat flow rate to be dissipated for the MHE and C_p is the specific heat of the fluid. Also, the heat flow rate for isothermal boundary condition should be:

$$\dot{Q} = hA \frac{(T_s - T_{out}) - (T_s - T_{in})}{\ln\left(\dfrac{T_s - T_{out}}{T_s - T_{in}}\right)}$$

From the last two equations an expression for the temperature leaving the channel can be found as:

$$T_{out} = T_s - (T_s - T_{in}) \exp^{\left(\frac{-nhA}{\dot{m} c_p}\right)}$$

where the product of hA is

$$hA = h(aL + 2Lb\,\eta_f)$$

The walls separating the channels are treated as fins with uniform rectangular cross section and insulated tips, where the fin efficiency can be expressed as:

$$\eta_f = \frac{\tanh(mb)}{mb}; \quad m = \sqrt{\frac{2h(L+s)}{k_{fin} L s}} \approx \sqrt{\frac{2h}{k_{fin} s}}$$

If T_{out} is different than $(T_{out})_{guess}$, $(T_{out})_{guess}$ is updated with T_{out} until convergence is achieved. The process is repeated until the error is less than a prescribed value.

The friction factor coefficient f for rectangular channels with laminar developed flow and non-slip flow can be calculated from the exact solution obtained from Shah and London [10].

$$f\,\mathrm{Re} = \frac{24}{\left(1+\dfrac{1}{\alpha}\right)^2 \left(1 - \dfrac{192}{\pi^5 \alpha} \displaystyle\sum_{n=1,3..}^{\infty} \frac{\tanh\left(\frac{n\pi\alpha}{2}\right)}{n^5}\right)}$$

which is closely approximated (within 0.05%) by the following empirical equation.

$$f\,\mathrm{Re} = 24(1 - 1.3553\alpha + 1.9467\alpha^2 - 1.7012\alpha^3 + 0.9564\alpha^4 - 0.2537\alpha^5)$$

In many applications, a major portion of the length is in developing flow. To account for the developing region, the pressure drop equation is presented in terms of an apparent friction factor.

$$\Delta p = \frac{2 f_{app} L \rho V^2}{d_h} = \frac{2 f L \rho V^2}{d_h} + K \frac{\rho V^2}{2}$$

where:

$$V = \frac{m_c}{\rho a b}$$

K represents the Hagenbach's factor for rectangular channels obtained by Steinke and Kandlikar [11].

$$K = 0.6796 + 1.2197\alpha + 3.3089\alpha^2 - 9.5921\alpha^3 + 8.9089\alpha^4 - 2.9959\alpha^5$$

All previous relations except the ones for Nu and T_{out} can be used for an isoflux boundary condition. The wall heat flux is found by dividing the heat flow rate by the product of wall area and number of channels.

$$q_{isoflux} = \frac{Q}{A\,n}$$

The Nusselt number and the temperature leaving the channel for isoflux rectangular channels can be expressed as:

$$Nu = 8.235(1 - 2.0421\alpha + 3.0853\alpha^2 - 2.4765\alpha^3 + 1.0578\alpha^4 - 0.1861\alpha^5)$$

$$T_{out} = T_s - \frac{q_{isoflux}}{h}$$

The third mathematical process shown in the flow chart is for the calculation of the pressure drop and entropy generation rate in the channel which will be explained in the next section.

Since the heat transfer and pressure drop are important parameters to calculate the entropy generation rate, the mathematical model for these parameters where validated. For this purpose, the proposed models for heat transfer and pressure drop were compared with Muzychka's models [12] that have been shown to be in excellent agreement with experimental data. The mathematical models are brought together in Figure 3 and good agreement is observed.

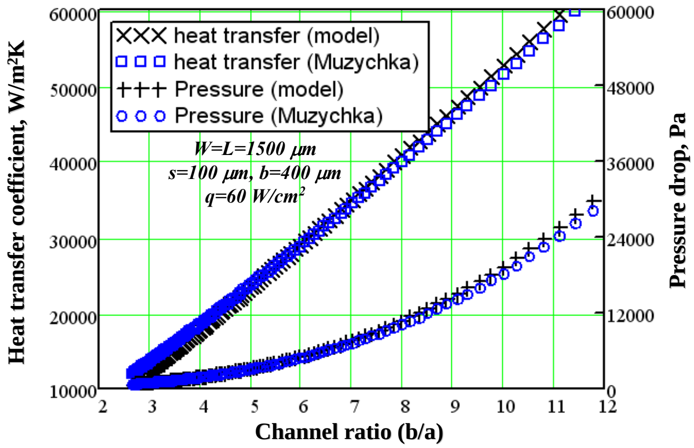

Figure 3: Heat transfer and pressure drop models comparison

ENTROPY GENERATION

Good heat exchanger design means, ultimately, efficient thermodynamic performance, that leads to a minimum generation of entropy or minimum destruction of the exergy in the system. The second law of thermodynamics states that all real-life processes are irreversible.

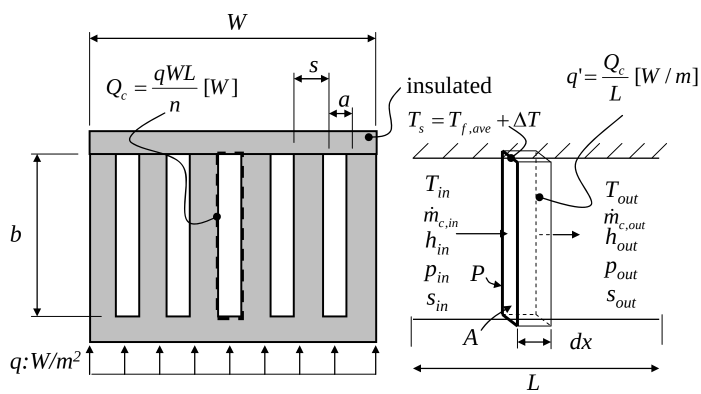

Figure 4: Control volume

As shown in Figure 4, a slice of thickness dx is considered as a control system. The second law of thermodynamics is applied to the system, and so the rate of entropy generation is given by Bejan [13]:

$$d\dot{S}_{gen} = \dot{m}ds - \frac{q'dx}{T_{ave,f} + \Delta T}$$

The first law of thermodynamics is applied to the same system:

$$\dot{m}\,dh = q'dx$$

In addition, considering the fluid as a homogeneous substance then:

$$\frac{dh}{dx} = T_{ave,f}\frac{ds}{dx} + \frac{1}{\rho}\frac{dp}{dx}$$

Combining the previous equations, the entropy generation rate per unit length can be written as:

$$\frac{d\dot{S}_{gen}}{dx} = \frac{q'\Delta T}{T_{ave,f}^{\ 2}(1+\tau)} + \frac{\dot{m}_c}{\rho T_{ave,f}}\left(-\frac{dp}{dx}\right)$$

where:

$$\tau = \frac{T_s - T_{ave,f}}{T_{ave,f}} = \frac{\Delta T}{T_{ave,f}}$$

Also the entropy generation rate can be related to the heat transfer coefficient and fluid friction, which were calculated in previous sections. After manipulations the entropy generation rate per unit length (per channel) can be expressed as:

$$\frac{d\dot{S}_{gen}}{dx} = \underbrace{\frac{q'^2}{4T_{ave,f}^{\ 2}(1+\tau)\dot{m}c_p}\frac{d_h}{St}}_{heat\quad term} + \underbrace{\frac{2\dot{m}_c^{\ 3}}{\rho^2 T_{ave,f}}\frac{f_{app}}{d_h A^2}}_{pressure\quad term}$$

The first term in the previous equation represents the entropy generation rate due to heat transfer (heat term), and the second the entropy generation rate due to viscous effects (pressure term). In order to illustrate the dependence of the Stanton number and friction factor, consider the case in which the heat transfer rate per unit length and mass flow rate are specified, it becomes evident that a high Stanton number contributes to the reduction of the entropy generation rate by heat, while high friction factor has the effect of increasing the entropy generation rate by pressure.

The problem considered in this study is to minimize the entropy generation rate given by the previous equation for a desired heat rate and channel depth. This approach allows the combined effects of thermal resistance and pressure drop to be assessed simultaneously as the MHE interacts with the surrounding field. The objective function is solved using the Generalized Reduced Gradient (GRF2) nonlinear optimization code.

CASE STUDIES AND DISCUSSIONS

The following case studies show the variation of the heat transfer coefficient, pressure drop and entropy generation rate with respect to some design parameters where the values are shown in Table 1. Six different channel depths ranging from 50 to 500 μm are simulated. For each depth the channel width is increased from 5 to 300 μm. This leads to a direct comparison of the effect of channel width on heat transfer, pressure drop, and entropy generation. Also, the effect of heat source size, channel wall thickness, and heat flux in the entropy generation rate were studied. The effect on heat source size was evaluated by changing the MHE width and length. The channel wall thickness effect was evaluated at two different wall thicknesses for the same MHE size.

Table 1: Design parameters and constants

Description	Parameter	Values
MHE width	*W*	*1.2,1.5,2.5 cm*
channel length	*L*	*1.2,1.5,2.5 cm*
channel width	*a*	*5 to 300 μm*
channel depth	*b*	*50 to500 μm*
channel wall thickness	*s*	*100, 200 μm*
heat flux	*q*	*20, 60, 90 W/cm^2*
maximum allowed chip temperature	T_{max}	*358 K*
coolant inlet temperature	T_{in}	*297 K*

The heat fluxes for the simulations (*20, 60, 90 W/cm^2*) were chosen based on the thermal design power (*TDP=130 W*[1]) and MHE dimensions. The wall temperature of the channel is assumed to be $T_s=358K$ (considered as the maximum allowable chip temperature). Water as coolant at $T_{in}=297\ K$ is assumed to enter into the microchannels.

An optimization method was used to identify the channel width which generates the lowest entropy generation rate for a given channel depth. Typical results using the proposed model for the entropy generation rate per unit length is shown in Figure 5 for a given channel depth, heat source power and size.

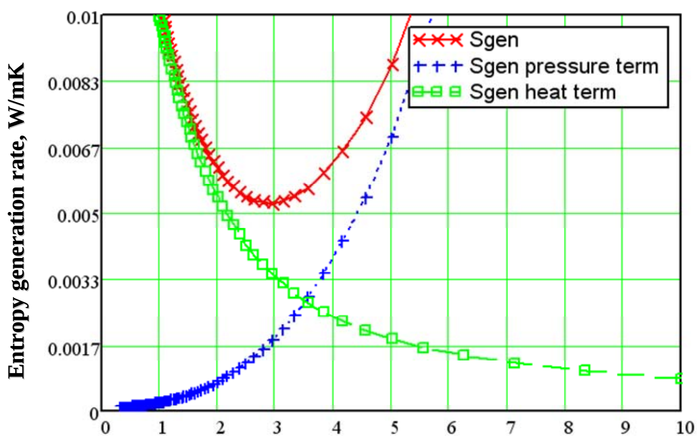

Figure 5: Entropy generation rate per unit length (pressure and heat terms)

From Figure 5, it is evident that increasing the channel aspect ratio by decreasing the channel width contributes to the reduction of the entropy generation rate by heat, while it has the effect of increasing the entropy generation rate due to viscous effects. This is because decreasing the channel size increases the pressure drop (entropy pressure term increases) and having smaller channel width allows for more channels within the fixed width (W) of the MHE, which reduces the heat transfer per channel (entropy heat term decreases).

[1] For Intel icore7 microprocessor TDP

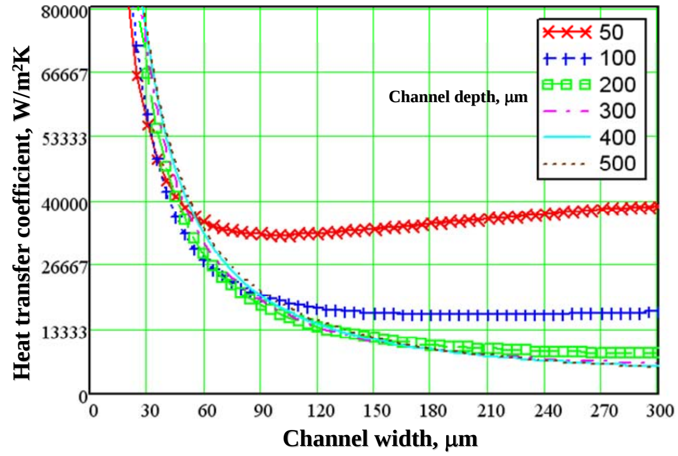

Figure 6: Heat transfer coefficient (isothermal)

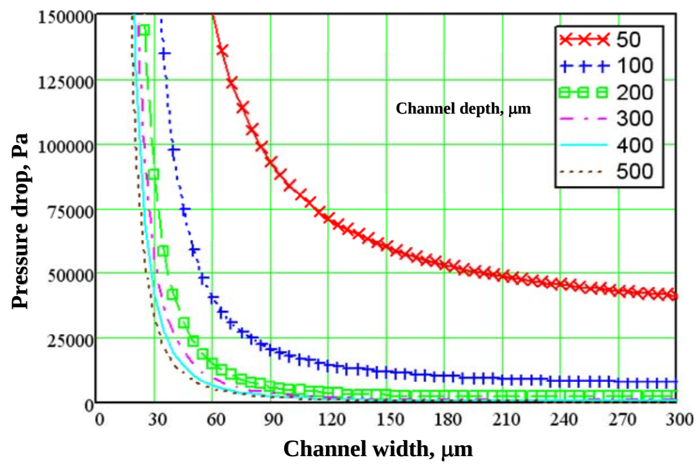

Figure 7: Pressure drop (isothermal)

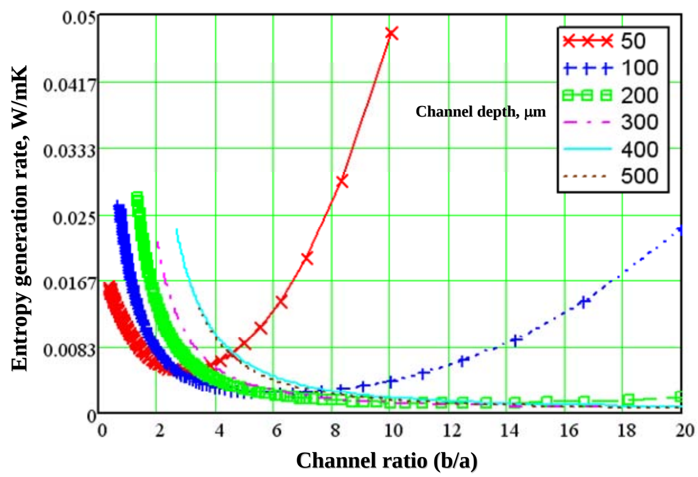

Figure 8: Entropy generation rate per unite length (isothermal)

The heat transfer, pressure drop, and entropy generation rates curves (per unit length) for a MHE with $W=L=1.5\ cm$, $s=100\ \mu m$, and heat flux $q=60\ W/cm^2$ are shown in Figures

6Figure 6-8 for the isothermal case and in Figures 9-11 for the isoflux boundary condition. The isoflux case showed higher heat transfer coefficient and pressure drop than the isothermal case. Since the heat transfer coefficient is directly proportional to the Nusselt number and the Nusselt number is greater for the isoflux boundary condition than the isothermal condition, this leads to a greater heat transfer coefficient for the isoflux case.

The heat transfer coefficient and entropy generation rate decrease with the channel width up to a minimum value before rising with the channel width.

Decreasing the channel size reduces the hydraulic diameter. Therefore, the heat transfer coefficient increases since it is inversely proportional to the hydraulic diameter. This is valid for a constant aspect ratio (*Nusselt=constant*: i.e. for aspect ratio 2 (see Figure 12), the heat transfer coefficient is higher for a channel 50 by 25μm than for a 500 by 250 μm). For aspect ratios below 1, where the Nusselt number decreases as the aspect ratio increases, the combined effect between Nusselt number and hydraulic diameter governs the changes in the heat transfer coefficient.

For all the case studies, the pressure drop was found to be higher for smaller and/or narrow channels as shown in Figure 13. The outlet temperature of the fluid was observed to be very close to the surface temperature for narrow channels. As the channels become more narrow, the outlet temperature increases. As the outlet temperature increases the mass flow rate required to carry away the specified amount of heat decreases. Also, since the width of each channel is decreased, the total number of channels increases. As a result the mass flow through each channel decreases. It may seem obvious to state that the pressure drop is directly proportional to mass flow per channel, however, the final assessment must consider the effects by the friction factor (proportional to pressure drop) and the hydraulic diameter (inversely proportional to pressure drop) as well. Therefore, these three variables govern the changes in pressure drop.

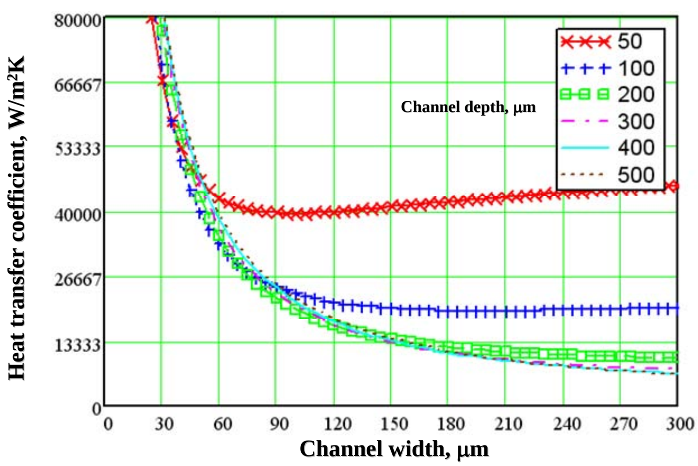

Figure 9: Heat transfer coefficient (isoflux)

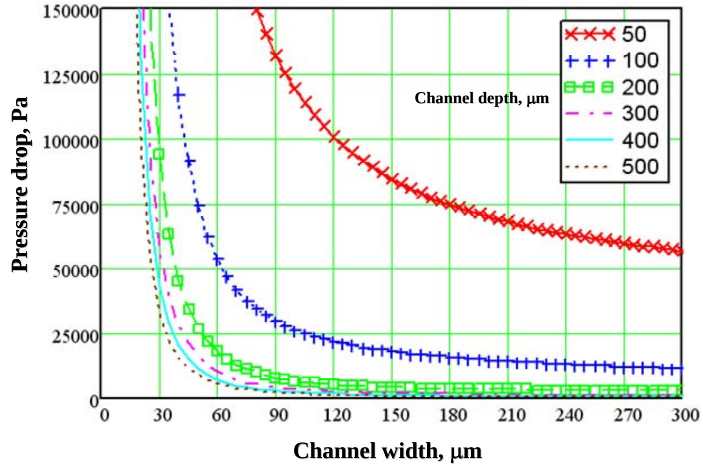

Figure 10: Pressure drop (isoflux)

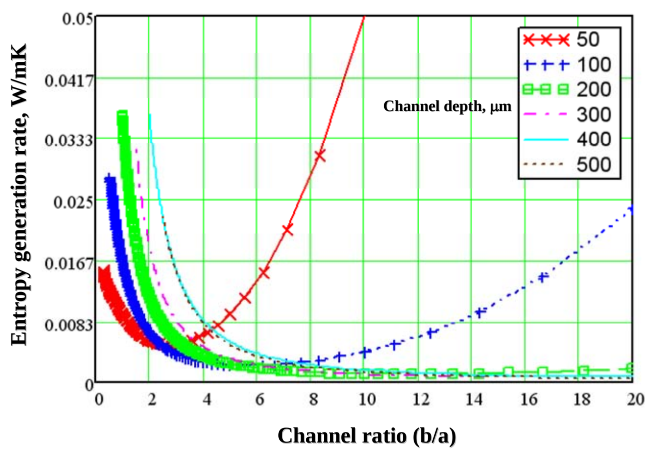

Figure 11: Entropy generation rate per unit length (isoflux)

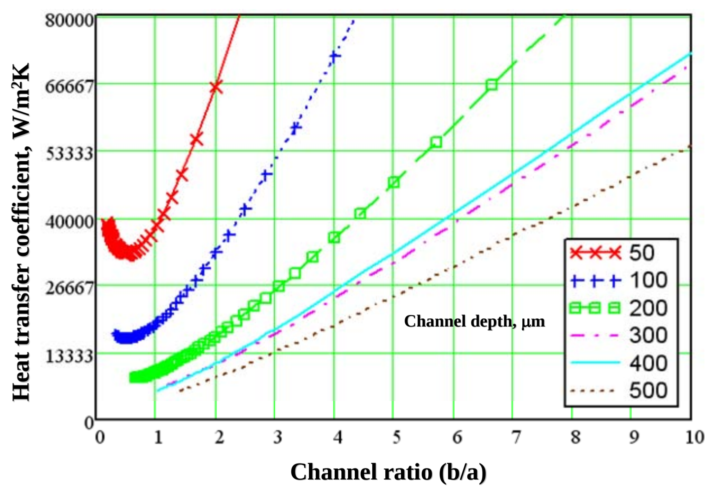

Figure 12: Heat transfer coefficient vs. channel aspect ratio (isothermal, q=60 W/cm^2)

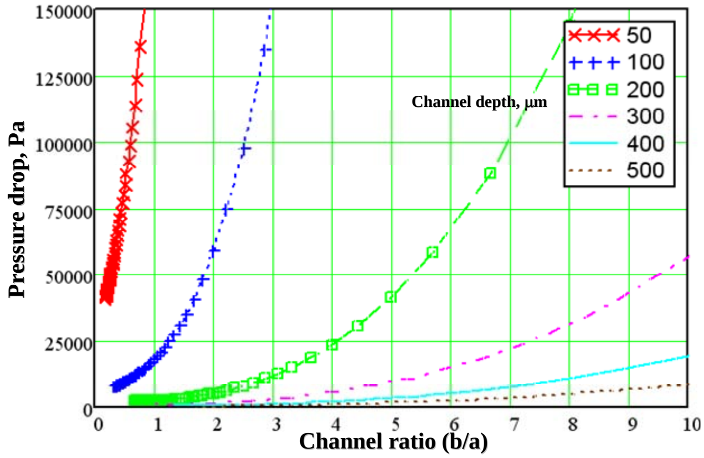

Figure 13: Pressure drop vs. channel aspect ratio (isothermal, q=60 W/cm^2)

The heat transfer coefficient needs to be considered in conjunction with the associated pressure drop. In this study both heat dissipation and pressure drop are considered simultaneously using entropy generation. The optimum channel is found based on the minimum entropy generation rate.

The optimum channel aspect ratio based on the minimum entropy generation rate for the 100 μm channel depth is located between 5 and 7 (see Figure 8 or Figure 11). Table 2 summarizes the optimum channel aspect ratio for depths between 50 and 500 μm (study case with $W=L=1.5$ *cm*, $s=100$ *μm*, $q=60$ *W/cm^2* and isotherm boundary condition). The Table 2 below is a list of different channel depths simulated with the mathematical model generating the optimum channel width which provides minimum entropy generation rate respectively. However, the least entropy generation rate occurs at the maximum channel depth during all the case studies which also corresponds to lowest pressure drop in the channel. Therefore, it can be concluded that the lowest entropy generation rate can be expected in deeper channels. This phenomenon is also observed in Figures 8 or 11.

Table 2: Optimum channel dimensions (isothermal)

b, μm	*h, W/m^{2}K*	*Δp, kPa [psi]*	*S_{gen} rate, W/mK*	*b/a*	*n, channels*
50	100,100	2020 [293]	5.253E-03	2.9	127
100	122400	1044 [151]	2.526E-03	6.3	128
200	135,400	494 [72]	1.214E-03	12.5	128
300	140,700	323 [47]	7.976E-04	18.8	128
400	134,600	202 [29]	5.934E-04	23.5	127
500	136,400	161 [23]	4.724E-04	29.4	127

Figure 14 shows optimum channel dimensions for different depths in a copper MHE for a chip size $W=L=1.5$ *cm* with $s=100$ *and* 200 *μm*, $T_s=358$ *K*, and water as the coolant with $T_{in}=297$ *K* at different heat fluxes.

For a particular channel depth, there is an optimum channel width which minimizes the entropy generation rate. As shown in Figure 14, the optimum aspect ratio is linearly proportional to the given channel depth regardless of the changes for the heat flux (q) and channel wall thickness (s). From the graph, for a given channel depth, the full range of heat fluxes and channel wall thicknesses coincide at a single point. Therefore, for a given channel depth, the optimum channel width has no relation with the heat flux and channel wall thickness with a given heat source size.

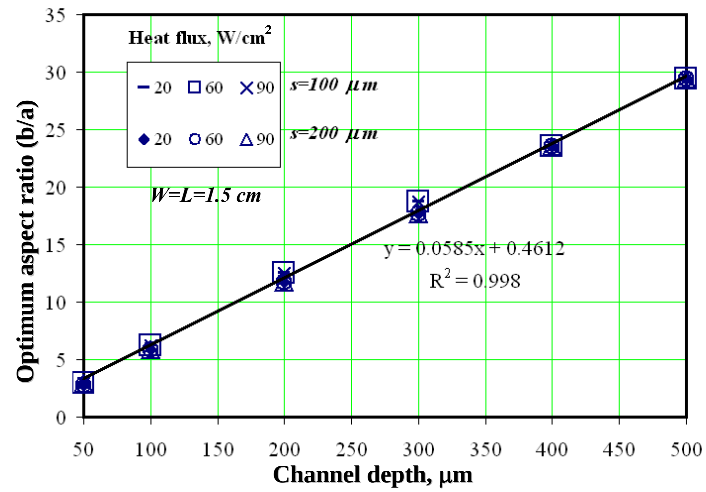

Figure 14: Optimum channel dimensions at different heat fluxes (*W=L=15 mm*, isothermal)

A further investigation is proposed related to a change in the wall thickness. Smaller wall thickness translates to more channels (n) at a specified MHE width. As illustrated in Figure 15, more channels show lower total entropy generation rate. Therefore, the designer has the option to choose for a configuration with the lowest entropy generation (better second law efficiency) or a configuration with fewer channels (easier manufacturability) but greater entropy generation rate. Also, it was found that the total entropy generation rate increases as the heat flux and/or wall thickness increases for a given heat source size.

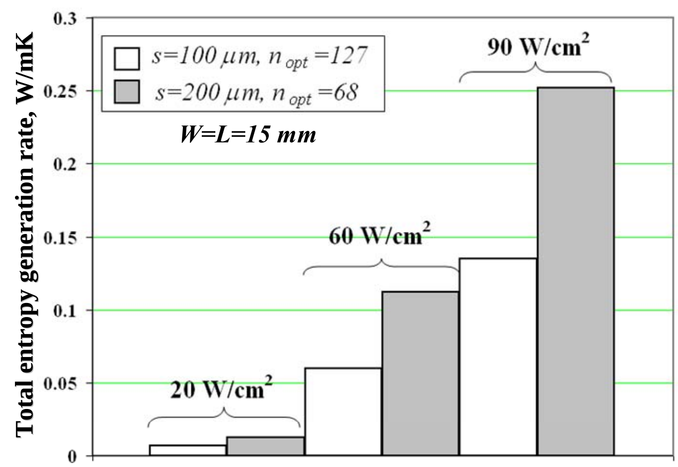

Figure 15: Effect of the heat flux and channel wall thickness on the total entropy generation rate per unit length

The effect of the chip size is evaluated for two square heat sources with 12 and 25 mm side as shown in Figure 16. Again the MHE is simulated as copper with the T_s=358 K, T_{in}=297 K, and a channel wall thickness of 200 µm.

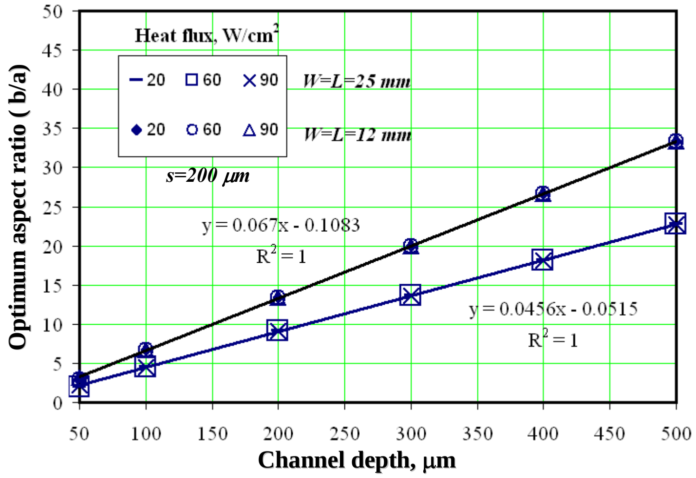

Figure 16: Optimum channel dimensions at different chip sizes (*s=200 µm*, isotherm)

This graph confirms the linear behavior between the optimum channel aspect ratio and the channel depth. However, as the heat source size increases the optimum channel aspect ratio decreases. Also note that for smaller channel depths the dependency of the optimum channel aspect ratio on heat source size becomes less significant. Thus, similar to the previous concluding statement at a given channel depth there is only one optimum aspect ratio for a particular heat source size.

Table 3 summarizes the optimum channel aspect ratio for depths 50, 60, 70, 80, 90 and 100 µm (case study with *W=L=1.5 cm*, *s=100 µm*, $q=100\ W/cm^2$, and isoflux boundary condition). The heat transfer coefficient for an isoflux condition is higher than the isothermal boundary condition, ranging between 5 and 10 %. Similarly, the pressure drop is higher for the isoflux case ranging between 2 to 16 %. Note that the optimum channel aspect ratios and number of channels for the isoflux and isotherm boundary conditions are very similar.

Table 3: Optimum channel dimensions (isoflux)

b, µm	*h, W/m² K*	*Δp, kPa [psi]*	*S_{gen} rate, W/mK*	*b/a*	*n, channels*
50	107,000	1755 [255]	5.069E-03	2.6	125
100	134,000	940 [136]	2.364E-03	5.9	127
200	144,300	430 [62]	1.135E-03	11.8	127
300	148,200	279 [40]	7.470E-04	17.6	127
400	150,300	206 [30]	5.569E-04	23.5	127
500	151,600	164 [24]	4.441E-04	29.4	127

While the optimization procedure estimates the optimum channel width (or channel aspect ratio), the relatively wide range of near minimum entropy generation rate as shown in Figure 17 (range between 13 to 21 on figure), provides designers with a range of options when specifying the appropriate channel width. This wide range of entropy generation was also reported by Culham and Muzychka [14] during the optimization of plate fin heat sinks using entropy generation minimization. A value closer to the maximum value in that range decreases the pressure drop in the microchannel, which may be beneficial when technical constrains are present in the design such as lower fluid pumping capacity.

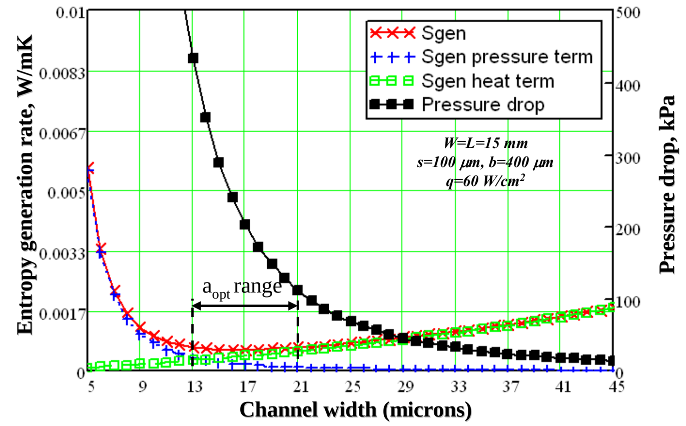

Figure 17: Range of near minimum entropy generation rate

Table 4 shows the decrease in pressure drop and increase in entropy generation rate in a MHE with *W=L=1500 µm*, *s=100 µm* and $q=60\ W/cm^2$ when the channel width is increased from the optimum value 17 µm to a near optimum channel width of 21 µm. The pressure drop is decreased up to 53 % and the entropy generation rate only increases up to 7 %.

Table 4: Changes on pressure and entropy generation rate near optimum channel width

b, µm	*a_{opt}, µm*	*a_{opt} range, µm*	*Δp, decreased, %*	*S gen, increased, %*
50	17	13-21	41	2
100	16	13-21	52	6
200	16	13-21	53	6
300	16	13-21	53	6
400	15	13-21	45	7
500	17	13-21	45	6

CONCLUSIONS

A procedure is presented that allows the channel width in a MHE to be optimized for a prescribe MHE size and channel depth. The procedure is based on the minimization of entropy generation resulting from viscous fluid effects and heat transfer for laminar and developed fluid flow. The optimum channel aspect ratio for the study cases shows a linear behavior with the channel depth, and similar results where observed for isothermal and isoflux boundary condition.

For a given channel depth and heat source size, the optimum channel aspect ratio remains constant regardless changes on the heat flux and/or channel wall thickness.

The optimization procedure estimates the optimum channel width for a particular channel depth but there is a relatively wide range of near minimum entropy generation rate. The designer may choose a channel width bigger than the optimum, which eventually increases the entropy generation rate by heat and decreases the entropy generation rate by viscous forces. This lower entropy generation by viscous forces is reflected by a lower pressure drop, which may be important for applications with fluid pumping limitations. In addition, choosing a channel width slightly bigger than the optimum and keeping constant the channel wall thickness requires less channels to be machined, which save time, tools, etc. during manufacturing.

For the analyzed MHE the optimum channel that minimizes the entropy generation seems to be narrow. Narrow channels were also reported in the literature as the ones that minimized the entropy generation rate.

There is an optimum channel width (or channel aspect ratio) that minimizes the entropy generation rate whereas thermal entropy generation rate increases and pressure drop decreases with increasing the channel width.

While the optimization procedure estimates the optimum channel width, the relatively wide range of near minimum entropy generation rate, provides designers with a range of options when specifying the appropriate channel width. These alternatives can lead to solutions where the pressure drop can be decreased without excessive increases in entropy generation.

The entropy generation rate has a strong relation with the number of channels and heat flux.

The heat transfer coefficient, pressure drop, and the entropy generation rate decrease with the channel width up to a minimum value before rising width the channel width.

ACKNOWLEDGMENTS

The authors gratefully acknowledge the financial support of the Ontario Graduate Scholarships and the Natural Science and Engineering Research Council of Canada.

REFERENCES

1. Khan, W. A., Yovanovich, M. M., and Culham, J. R., 2006, *"Optimization of Microchannel Heat Sinks Using Entropy Generation Minimization Method"*, Twenty-Second Annual IEEE Semiconductor Thermal Measurement and Measurement Symposium, Dallas, TX, USA.
2. Chen, K., 2005, *"Second-law Analysis and Optimization of Microchannel Flows Subjected to Different Thermal Boundary Conditions"*, International Journal of Energy Research, 29(3), pp. 249-63.
3. Abbassi, H., 2007, "*Entropy Generation Analysis in a Uniformly Heated Microchannel Heat Sink*", Energy 32, pp.1932-1947, doi:10.1016/j.energy.2007.02.007.
4. Zheng, X., and Silber-Li, Z., 2008, *"Measurement of Velocity Profiles in a Rectangular Microchannel with Aspect Ratio α=0.35"*, Experiments in Fluids, 44(6), pp. 951-959, doi:10.1007/s00348-007-0454-4.
5. Papautsky, I., Ameel, T., and Frazier, A., 2001 *"A Review of Laminar Single-phase Flow in Microchannels"*, ASME International Mechanical Engineering Congress and Exposition, Proceedings, Vol. 2, pp. 3067-3075.
6. Papautsky, I., Gale, B., K., Mohanty, S, Ameel, T., A., and Frazier, A., B., 1999, *"Effects of Rectangular Microchannel Aspect Ratio on Laminar Friction Constant"*, Proceedings of SPIE-The International Society for Optical Engineering, Vol. 3877, pp. 147-158,
7. Park, H., S., and Punch, J., 2008, *"Friction Factor and Heat Transfer in Multiple Microchannels with Uniform Flow Distribution"*, International Journal of Heat and Mass Transfer, 51(17-18), pp. 4535-4543, doi:10.1016/j.ijheatmasstransfer.2008.02.009.
8. Kakac, S., Shah, R., K., and Aung, W., 1987, *"Handbook of Single Phase Convective Heat Transfer"*, John Wiley & Sons, Inc., New York.
9. Upadhye, H., R., and Kandlikar, S., G., 2004, "*Optimization of Microchannel Geometry for Direct Chip Cooling Using Single Phase Heat Transfer*", Proceedings of the Second International Conference on Microchannels and Minichannels (ICMM2004), pp. 679-685.
10. Shah, R., K., and London, A., L.,1978, *"Laminar Flow Forced Convection in Ducts"*, Supplement 1 to Advances in Heat Transfer, Academic, New York.
11. Steinke, M., E., and Kandlikar, S., G., 2006, *"Single Phase Liquid Friction Factors in Microchannels"*, International Journal of Thermal Sciences, 45(11), pp. 1073-1083
12. Muzychka, Y., 1999, *"Analytical and Experimental Study of Fluid Friction and Heat Transfer in Low Reynolds Number Flow Heat Exchangers"*, PhD thesis, Department of Mechanical Engineering, University of Waterloo.
13. Bejan, A., 1996, *"Entropy Generation Minimization*", CRC press, Inc., New York.
14. Culham, J., R., and Muzychka, Y., S., 2001, *"Optimization of Plate Fin Heat Sinks Using Entropy Generation Minimization"*, IEEE Transactions on components and packaging technologies, Vol. 24, No.2, pp. 159-165.

